CHAPTER 2

Cavity-enhanced absorption spectroscopy of plasma jets

The different laboratory spectroscopic techniques used in this thesis are presented in this chapter. The concept of absorption spectroscopy is introduced, where the basic requirements needed to record a spectrum are laid out. The two methods employed here, known succinctly as IBBCEAS and CRDS, both utilize an optical cavity which greatly enhances the sensitivity in detecting short-lived and reactive molecules. In the context of this thesis, the former is best used in making a survey for [new] spectral features, as it is fairly sensitive and can cover a wide wavelength range in a short amount of time for each measurement run, while the latter, offering a much higher spectral resolution, is utilized in zeroing-in on these absorption features to further unravel structural details. From a precursor gas mixture, the chemical species of interest are synthesized using plasma nozzles which produce supersonic jets of radicals and ions in the gas phase. Here, several conceptually different plasma nozzle systems will be described. Species formed in the resulting plasma expansions can be identified using, for example, rotational constants and vibronic energy differences which can be obtained by analyzing the recorded spectra. Searching in the laboratory for potential carriers of unidentifiable features from astronomical surveys, such as the diffuse interstellar bands, can thus be efficiently implemented using IBBCEAS and CRDS—two complementary measurement schemes that will be described shortly.

This chapter forms the basis for work currently prepared for publication.

2.1 Introduction

The basic ingredients for a direct spectroscopic absorption experiment include a source of radiation, a light-dispersing medium for generating a spectrum, an absorbing material (i.e., the sample to be analyzed), and a detector. The Beer-Lambert (or Beer-Lambert-Bouguer) law for the absorption of light states that the higher the concentration of the sample and the longer the path that light travels through it, the more the light gets absorbed.[1] For a particular measurement a high signal-to-noise ratio (S/N) can be obtained by increasing the sample density and/or the effective absorption pathlength; this, however, is not always possible. One practical solution would be to contain the sample inside an optical cavity (the absorption cell) and have the light pass through the sample more than once. Mirror configurations that allow for multipass absorption already exist – the Pfund cell (invented by August Pfund in the late 1930s), the White cell (White 1942), the Herriott cell (Herriott & Schulte 1965), the circular multipass cell (Thoma et al. 1994), and other variations that rely on precise laser beam patterns on the mirrors (Kaur et al. 1990, McManus et al. 1995) – and these have their own utility depending on the application and/or the design constraints of the experiment. These are typically challenging to set up, since they require that the light beams be spatially separated which consequently demand larger mirrors, and some have mirror holes precisely aligned to let the light in or out. With the advent of mirror coating techniques (e.g., evaporative deposition, ion-beam sputtering)[2] that can achieve reflectivities of more than 99.9%, an optical cavity can now be constructed with only two mirrors sharing a single optical axis which simplifies the configuration and alignment procedure. Light enters the cavity through one of the cavity mirrors and exits through the other. The high reflectivity essentially enables the light to be trapped in between the two mirrors for a much longer time, and thus for a much longer total travel path. If an absorbing sample is contained in this cavity, the total absorption from the injected light is compounded significantly as the trapped light bounces back and forth through the sample. Using this technique, a typical sample length of a few centimeters can have an effective absorption path length of up to a few kilometers. This is the basic concept behind cavity-enhanced absorption spectroscopy (CEAS). (For a comprehensive review of the principle and development of CEAS and its various techniques, see, e.g., Berden et al. 2000, Berden & Engeln 2009, Romanini et al. 2014.)

---

[1] $A = \sigma(\lambda)nl$, where A is the absorbance, $\sigma(\lambda)$ is the absorption cross section [cm^2] of the sample for a particular wavelength λ, n is the number density [cm^{-3}], and l is the pathlength of light through the sample [cm]. This linear relationship only holds true for as long as the absorption is small enough so as not to cause optical saturation which can lead to stimulated emission.

[2] Traditionally, through the process of 'silvering', a thin coat of metal such as aluminum, copper, silver, or gold is applied onto a glass substrate, producing mirrors with average reflectivities of 80–99% in the visible region.

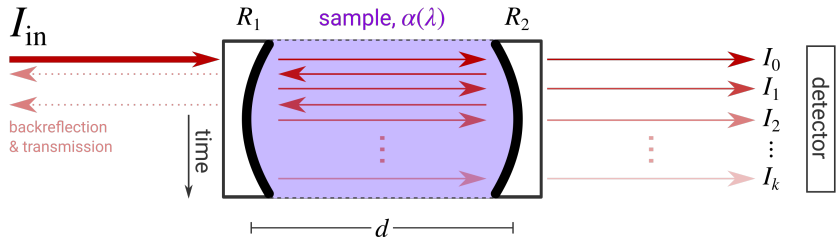

Figure 2.1: Schematic of the CEAS configuration. In reality, the light rays lie along the optical axis of the cavity; they are separately drawn to denote their temporal evolution.

2.2 Cavity-enhanced absorption spectroscopy

When monochromatic light of intensity I_{in} passes through a sample of length l with a wavelength-dependent absorption 'strength' denoted by the coefficient $\alpha(\lambda)$, the output intensity I_{out} follows

$$I_{out} = I_{in}\, e^{-\alpha(\lambda)l}, \tag{2.1}$$

which is assumed to be within the linear regime of the Beer-Lambert law. As was described above, the absorption can be enhanced by containing the sample in a stable optical cavity comprised of two mirrors, each with reflectivities R_1 and R_2 separated by a distance d. Although the sample may span the whole length of the cavity ($l = d$), in some cases as with the supersonic plasma jets studied in this thesis, $l < d$; the former is adopted for simplicity in the formulation.

Figure 2.1 depicts a schematic of the CEAS multipass configuration. After the first pass through the sample, the light intensity detected at the exit end of the cavity is

$$I_0 = I_{in}(1 - R_1)\, e^{-\alpha d}(1 - R_2). \tag{2.2}$$

The terms $(1 - R_1)$ and $(1 - R_2)$ set the fraction of light transmitted through each of the mirrors. It is assumed here that other loss mechanisms, such as absorption and scattering in the mirror substrate and the sample container walls, are much smaller than what is limited by the mirror reflectivities. The first internally-reflected light inside the cavity will have an intensity equal to $I_{in}(1 - R_1)\, e^{-\alpha d} R_2$, and will further take a factor of $e^{-\alpha d} R_1 e^{-\alpha d}(1 - R_2)$ after completing one round-trip (two passes). It is straightforward to show that for each round-trip until the kth time following the first pass, the detected intensity becomes

$$
\begin{aligned}
I_1 &= I_{\text{in}}(1-R_1)\,e^{-\alpha d}R_2e^{-\alpha d}R_1e^{-\alpha d}(1-R_2)\\
I_2 &= I_{\text{in}}(1-R_1)\,e^{-\alpha d}R_2e^{-\alpha d}R_1e^{-\alpha d}R_2e^{-\alpha d}R_1e^{-\alpha d}(1-R_2)\\
&\vdots\\
I_k &= I_{\text{in}}(1-R)^2\,e^{-\alpha d}\left(Re^{-\alpha d}\right)^{2k} = I_0\left(Re^{-\alpha d}\right)^{2k},
\end{aligned}
\tag{2.3}
$$

with R as the 'effective' reflectivity equivalent to the geometric[3] mean $\sqrt{R_1R_2}$. From this it is clear that for a particular sample the enhancement of the absorption solely depends on the mirror reflectivities, as this determines the number of passes achievable. For an empty cavity (i.e., $\alpha = 0$), Eq. 2.3 becomes $I_k = I_{\text{in}}(1-R)^2R^{2k}$. To obtain a spectrum, the detected[4] intensity of light transmitted through the cavity with and without an absorbing medium is compared, and is then plotted with the wavelength of light. The two CEAS methods used in this thesis, namely Incoherent BroadBand Cavity-Enhanced Absorption Spectroscopy (IBBCEAS) and Cavity Ring-Down Spectroscopy (CRDS), can be distinguished by how these detected intensities of light are handled and analyzed. Each technique will be described in the succeeding sections.

2.2.1 Incoherent broadband CEAS

The principle of Incoherent BroadBand Cavity-Enhanced Absorption Spectroscopy (IBBCEAS) was first developed and demonstrated by Fiedler et al. (2003) (see also Fiedler 2005 and references therein for a detailed theory on the discussion below). In this method, incoherent broadband light is coupled into the optical cavity, and the transmitted light is integrated through the detector. Although the formulation above was made for monochromatic light, this can readily be extended to all frequencies in accordance to the superposition principle. For each wavelength λ, the total detected intensity is the sum of all transmissions through the exit mirror, that is,

$$
I_{\text{out}} = \sum_{k=0}^{\infty} I_k = I_{\text{in}}(1-R)^2\,e^{-\alpha d}\sum_{k=1}^{\infty}\left(Re^{-\alpha d}\right)^{2k}. \tag{2.4}
$$

With $R \to 1$ the summation converges and Eq. 2.4 can be expressed as

$$
I_{\text{out}} = I_{\text{in}}\frac{(1-R)^2e^{-\alpha d}}{1-\left(Re^{-\alpha d}\right)^2}, \tag{2.5}
$$

[3] Compared to the arithmetic mean, taking the geometric mean will prevent the larger of the two reflectivities to dominate the 'effective' value. *Source*: `https://www.landonlehman.com/post/the-geometric-mean/` (accessed on 8 April 2019).

[4] The attenuated signal after the kth round-trip should be above the noise level of the detector.

and for an empty cavity,

$$I_{\text{out}}^{0} = I_{\text{in}} \frac{1-R}{1+R}. \tag{2.6}$$

These intensities are measured simultaneously for each wavelength dispersed at a given moment, and a spectrum is generated by taking the ratio of the detected intensities with and without the absorbing medium. The spectral resolution, largely determined by the monochromator used in dispersing the light, is moderate compared to laser-based techniques such as CRDS (Sec. 2.2.2). However, in the case of diffuse interstellar bands research, the somewhat lower spectral resolution is no issue, as DIBs tend to be broad and unresolved. In addition, a substantially wider spectral coverage can be achieved with IBBCEAS for a much shorter measurement time since less reflective mirrors are used (compared to those in CRDS) which can be manufactured with a wider bandwidth.

The IBBCEAS setup (Figs. 2.2 and 2.3; also known as the BroadBand – Diffuse Interstellar Bands setup or BB-DIB; Walsh et al. 2013) in the Sackler Laboratory for Astrophysics at Leiden Observatory is comprised of, first and foremost, a 300-W xenon arc lamp (LOT, LSB530; Ushio, UXL-302-0) which simultaneously provides light across the entire visible spectrum, with an extended coverage towards the UV and the near-IR region (200 nm – 2.5 μm). This light is collimated through a telescope assembly and coupled into an optical cavity (with two mirrors of $R \gtrsim 99.95\%$) that contains the absorbing material; typically a hydrocarbon plasma jet is positioned. (Details on the production of the pulsed plasma jet will be described in the subsequent sections.) Light leaking out of the cavity is collected by means of a circular-to-rectangular fiber optic bundle (LOT, LBB552) that directs it through the entrance slit (13 μm) of a Czerny-Turner-type spectrograph (Andor, Shamrock 750). Inside the spectrograph, a grating (1800 lines/mm; spectral resolution of 0.03 nm) held on a turret disperses the light and projects a wavelength range of 20 nm at a time onto a charge-coupled device (CCD) array (Andor, Newton) of 2048×512 pixels. The pixels provide an absolute wavelength accuracy of 0.1 Å which is sufficient for comparing with the best-resolved DIB features. To record a spectrum, the light reaching the CCD is integrated over time using various settings for exposure, readout rate, number of accumulated exposures, etc., depending on the application while also avoiding saturation of the pixels and the A/D converter. Typically, every column of CCD pixels is binned together to generate a one-dimensional spectrum of photoelectron counts versus the wavelength of light. After each measurement of an absorption signal, a reference spectrum is taken without the plasma jet which is used for subtracting/dividing the lamp and cavity transmission continuum from the signal. Wavelength calibration is made possible by separately recording an emission spectrum from a mercury or sodium discharge lamp. In addition, atomic emission lines (e.g., Ar^{+}) from the plasma glow, if present, can also be used for this purpose. An interference filter is placed before the fiber optic bundle to further block off most of the emitted light from the plasma (and the Xe arc lamp) that is outside the wavelength range for which the cavity mirrors

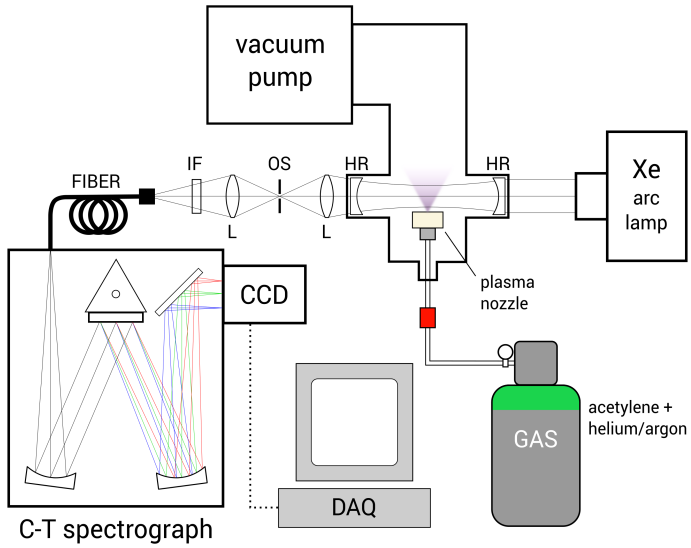

Figure 2.2: Block diagram of the IBBCEAS setup at the Sackler Laboratory for Astrophysics in Leiden. High-reflectivity mirror (HR); lens (L); optomechanical shutter (OS); interference filter (IF); Czerny-Turner (C-T) spectrograph; charge-coupled device (CCD); data acquisition interface (DAQ).

have R-values above 99.95%. The mirrors used (e.g., Research Electro-Optics Inc., Layertec) typically only offer less than 100 nm of wavelength bandwidth, and thus, was replaced accordingly to cover as much of the visible spectrum.

It should be noted that the lamp produces continuous-wave (cw) radiation whereas the plasma jet comes in 1–2-ms pulses at 25 Hz. This means that an absorption signal can only be present whenever light coincides in time with the plasma jet, and so, the CCD also gets exposed to light that does not contain any signal at all (the data acquisition duty cycle is much less than one). As a consequence, the S/N lowers and the sensitivity of the measurement decreases. To mitigate this, the light transmitted through the exit mirror of the cavity is focused through the slot of an optomechanical shutter (Stanford Research Systems, SR540) that is synchronously referenced to the repetition rate of the plasma pulse to cut off the light which does not carry any spectral information. Furthermore, the CCD is cooled using a thermoelectric cooler (bringing its temperature down to –70°) to minimize the electronic noise due to its inherent dark current.

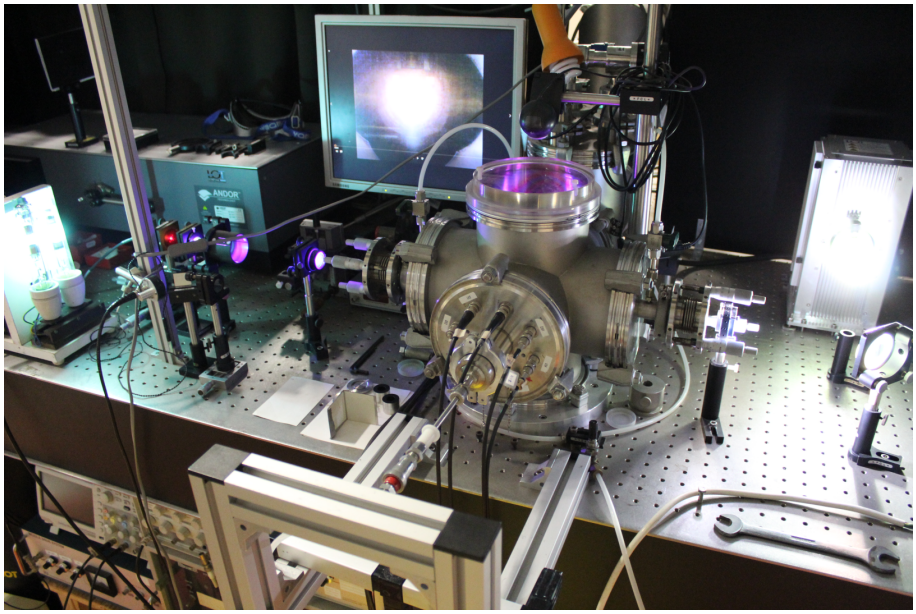

Figure 2.3: The BB-DIB setup in the Sackler Laboratory for Astrophysics at Leiden Observatory.

2.2.2 *Cavity ring-down spectroscopy*

The other technique known as [pulsed] Cavity Ring-Down Spectroscopy (CRDS), first demonstrated by O'Keefe & Deacon (1988), employs a laser which can be tuned across a certain wavelength range. Instead of integrating the intensity of the exiting light as in IBBCEAS, its attenuation is measured in time as it bounces from one to the other mirror (Fig. 2.4). Building from the previous formulation in Sec. 2.2, it can be shown that the time t elapsed for k round-trips is $t = 2dk/c$, where c is the speed of light. Equation 2.3 can now be expressed as

$$I(t) = I_0 \exp\left[\frac{ct}{d}\left(R - 1 - \alpha d\right)\right]. \tag{2.7}$$

The intensity of light decays exponentially, hence the term 'ring-down'. The time when I_0 has decreased by a factor of $1/e$ is the characteristic ring-down time τ which is defined as

$$\tau = \frac{d}{c(1 - R + \alpha d)}, \tag{2.8}$$

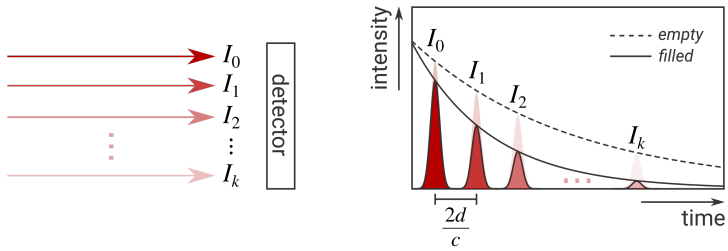

Figure 2.4: *Continued from Fig. 2.1.* The exponential decrease in light intensity is measured in CRDS. (The roundtrip time for one laser pulse is equal to twice the cavity length d divided by the speed of light c.) The ring-down time for light in a cavity with an absorbing sample decays faster than for an empty one; this characteristic time is determined and plotted for each wavelength to obtain an absorption spectrum.

and for an empty cavity,

$$\tau^0 = \frac{d}{c(1-R)}. \tag{2.9}$$

Equation 2.9 can be used for accurately calculating mirror reflectivities, as was done in the first conceptualization of the CRD technique (Crawford 1985). To extract the ring-down time, a mono-exponential decay curve is fitted to the recorded ring-down transient. In this way CRDS can also be used for recording absorption signals. An absorption spectrum is obtained by taking the ratio of ring-down times with and without the sample and plotting it for each wavelength. The spectra are recorded at a high resolution which allows for the determination of accurate molecular parameters. Since the decay rate, rather than the absolute intensity, is measured, CRDS is insensitive to power fluctuations for each input light pulse. This is crucial since it is preferred to have experimental conditions as constant as possible for the whole measurement run where it typically takes a much longer time to obtain a wavelength scan compared to, e.g., IBBCEAS. However, since CRDS requires higher mirror reflectivities (typically, in the experiments performed in this thesis, $R \gtrsim 99.995\%$), this consequently limits the range of wavelengths that can be covered for a given measurement. Similarly, the lasing frequency of the dye is another limiting factor to consider when using a dye laser as a light source. Due to this inherent slowness especially when larger wavelength domains have to be covered, combining CRDS with IBBCEAS makes for a viable experimental approach in tackling spectral identification of astronomical observations such as the carriers of the DIBs.

In the LaserLaB at the Vrije Universiteit Amsterdam, a standard pulsed-CRDS setup (Ityaksov 2009, Zhao et al. 2011a, Haddad 2014, Bacalla et al. 2015) is used for recording spectra of transient species in the gas phase produced in a plasma discharge

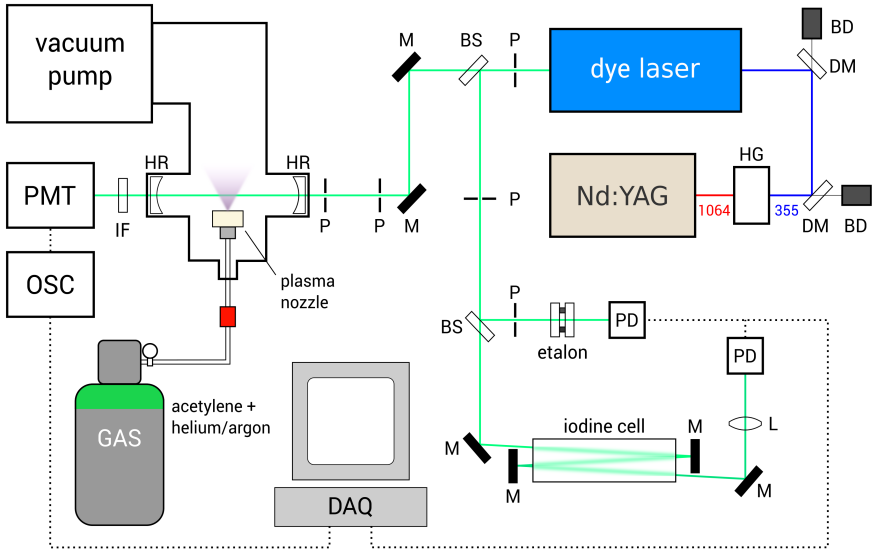

Figure 2.5: Block diagram of the CRDS setup in the LaserLaB in Amsterdam. Harmonic generation crystal (HG); dichroic mirror (DM); beam dump (BD); pinhole (P); beamsplitter (BS); lens (L); photodiode (PD); mirror (M); high-reflectivity mirror (HR); interference filter (IF); photomultiplier tube (PMT); oscilloscope (OSC); data acquisition interface (DAQ). *Figure adapted from* Bacalla (2014).

(Figs. 2.5 and 2.6). The light source is a tunable dye laser (Sirah, Cobra-Stretch) pumped by a Nd:YAG laser (Laser Physics, Quanta-Ray). Different dyes can be used, offering specific bandwidths across the IR-Vis-UV range, which can be pumped with either 532- or 355-nm light that is harmonically generated from the 1064-nm light of the Nd:YAG. The laser is typically operated at a 10-Hz repetition rate with a pulse width of around 6 ns at 66 mJ per pulse. Lasing from the dye can be narrowed down to a bandwidth of 0.035 cm^{-1} by using its 2nd order diffraction from two gratings (in a Littrow configuration) which serve as the wavelength selector. The laser beam is split into two: one is directed to the ring-down cavity while the other goes to the calibration section of the setup. A photomultiplier tube (PMT) records the ring-down signal and an interference filter is placed in front of the PMT to filter out the light from the glow produced by the plasma discharge. While taking the ring-down signal, étalon fringes are also recorded together with an absorption spectrum of iodine gas in a cell. The fringes are used for correcting any non-linearity in the wavelength scan brought about by the mechanical tuning of the wavelength selector; the I_2 spectrum

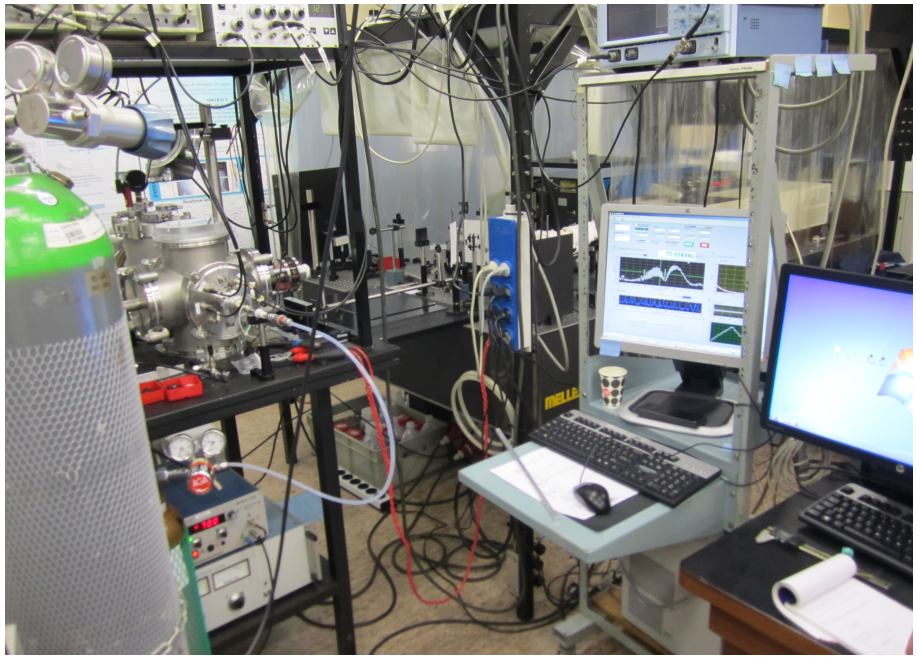

Figure 2.6: The pulsed-CRDS setup in the LaserLaB at the VU University Amsterdam.

($\sim$ 11 600–20 000 cm^{-1} or $\sim$ 500–860 nm) is for absolute wavelength calibration, with an accuracy of $\pm$ 0.02 cm^{-1} (Martin et al. 1986, Knöckel et al. 2004). The ring-down signal from the oscilloscope, as well as the étalon transmission and I_2 absorption signals from the photodetectors, are interfaced into a computer where data are recorded and analyzed. Using a routine developed in LabVIEW, an exponential decay curve is fitted to the ring-down signal and a data point is recorded for every average of 10 ring-down events. In this setting, a measurement covering $\sim$ 10 cm^{-1} (0.3 nm) will run for about an hour. Wavelength calibration is performed in the PGOPHER software (Western 2014), as well as the absorption line / band fitting to extract molecular constants from the recorded spectrum.

2.3 Plasma production

In this work, the spectra of carbon-based molecules in the gas phase are studied. The molecular transients are formed in supersonically expanding plasma jets. The basic idea is to start with a dilute mixture of a precursor gas and an inert buffer gas: $<$ 1% acetylene (C_2H_2) in helium or argon. The gas mixture is injected into the vacuum chamber (baseline pressure in the order of 10^{-3} mbar) through a solenoid valve (General Valve, Series 9) with a 2-mm orifice and is typically operated at a pulse du-

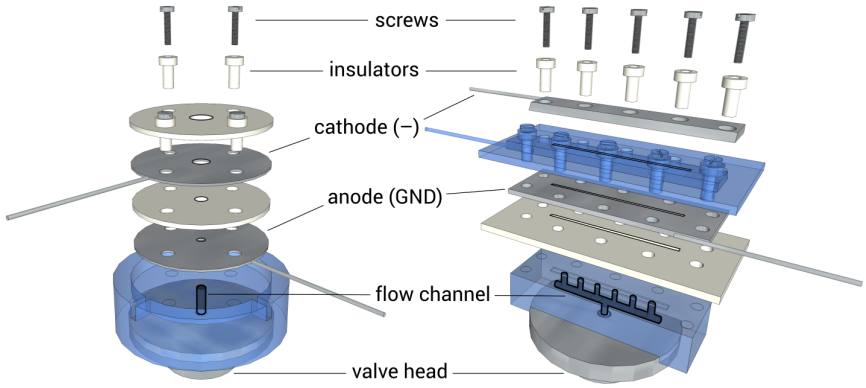

Figure 2.7: Exploded view drawing of the pinhole- and slit plasma nozzle. In essence, both designs incorporate metal- and ceramic plates arranged alternately—the main difference being the profile of the generated plasma jet (conical and planar, respectively). Some components in the figure are set as transparent (blue) for visual aid.

ration of around 1 ms. Behind the solenoid a gas flow fixture with a pinhole or slit is mounted. A rotary vane – roots blower pump system ($\sim$ 1000 m^3/h pumping capacity) is used for maintaining the vacuum pressure at around 0.1 mbar as the gas expands supersonically into the chamber. Aside from reduced gas use, in contrast to a continuous gas flow, operating in pulsed-mode helps in attaining higher input/backing pressures (up to 10 bar) which enhances the rotational/vibrational cooling of the molecules due to the adiabatic expansion of the gas into the vacuum chamber. This is important since the rovibrational temperature will affect the profile of the spectrum and thus, the low-temperature spectra makes it easier to directly compare the recorded features in the laboratory with astronomical spectra. Moreover, as a limited number of molecules is forced into a smaller number of states, the overall detection sensitivity increases.

To generate the plasma, a stream of electrons is needed to break apart the precursor molecules into smaller units which can then recombine to form larger species such as carbon chains. The manner as to how this final step is done sets the different nozzle configurations apart from each other, and this will be described in detail below.

2.3.1 Pinhole- and slit nozzle

The pinhole- and slit nozzle both consist of metal plates that are separated by a ceramic insulator, with the whole assembly fastened onto a certain type of gas flow channel piece that sits atop the solenoid valve head (Fig. 2.7). The plate situated most downstream is raised to a high negative voltage (cathode) with respect to a grounded

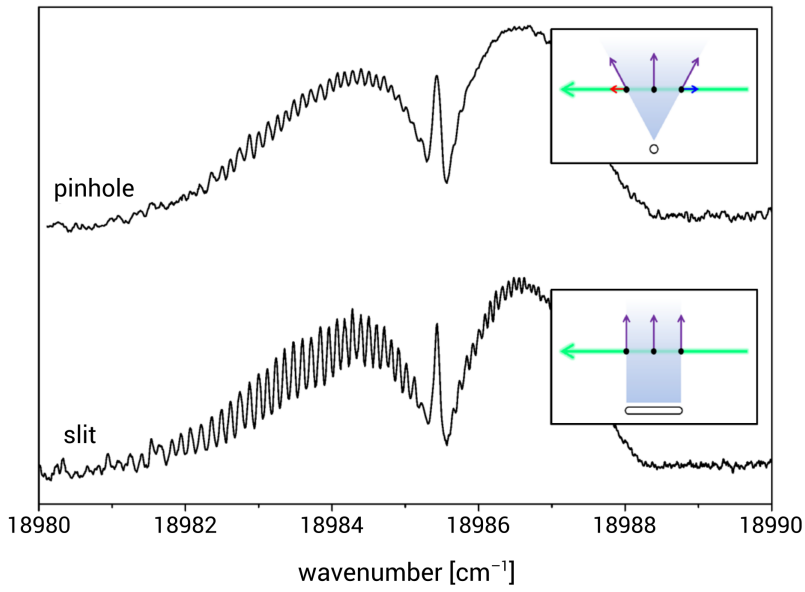

Figure 2.8: Comparison of the plasma jet profiles produced (inset) and the resulting spectra using a pinhole and a slit nozzle. Since velocity components (red and blue arrows) along the optical axis of the cavity (green arrow) are minimized in a planar plasma expansion, the resulting absorption line widths in the spectrum recorded are narrower / more resolved, that is, Doppler broadening is reduced. The spectrum shown here is a spin-orbit component ($\Omega = 3/2$) of the $B^2\Pi_\Omega - X^2\Pi_\Omega$ electronic origin band of C_6H, measured with CRDS. *Figure taken from* Bacalla (2014).

plate, creating a potential difference that allows for electrons to jump from one plate to the other as the gas pulse comes in between. Voltages from -600 to -1000 V are typically used, and currents of up to 120 mA are needed to keep the plasma stable. The plates are arranged such that the electrons will flow counter to the gas flow (i.e., upstream) so as to increase the efficiency in dissociating the molecules. In fact, this is the only configuration that allows a stable flow as otherwise the much slower cations are forced upstream. Similarly, this electron discharge is pulsed and is synchronized together with the injection of the gas into the vacuum chamber—the discharge ideally going off at the most concentrated and stable part of the gas pulse. The plasma interaction region in the space between the plates is where most of the recombination of dissociated fragments occurs; high backing pressures also increase the instances of collisions in this confined space.

The main difference between the pinhole- and the slit nozzle design, as their names suggest, is the form of the nozzle orifice which consequently affects the result-

ing geometry of the plasma jet. The pinhole design, comprised of alternating metal- and ceramic plates with holes of increasing diameter (1.0–3.5 mm), produces a conical plasma expansion profile with a particle density that decreases quadratically with distance from the nozzle along the gas flow direction (downstream). On the other hand, the slit design is formed by an array of pinholes that distribute the gas output along a line, providing for a longer sample length. Particularly in combination with CRDS or IBBCEAS, this increases the effective absorption pathlength. Combined with plates of narrow slit orifices (3 cm $\times$ 200–800 μm), this nozzle also effectively generates a planar plasma expansion which significantly reduces the first-order Doppler broadening of the absorption lines (Fig. 2.8). Downstream, the particle density of the planar plasma decreases inversely with distance from the nozzle. In addition, instead of having a single cathode, the slit nozzle has two metal jaws with which the separation distance can be adjusted. This can narrow down the jet expansion angle perpendicular to the slit orientation and will further increase the collision-induced cooling of rovibrational states of the molecules. Finally, the pinhole nozzle consumes much less gas than the slit which makes it a better choice when recording the spectra of plasma synthesized using [expensive] isotope precursors.

2.3.2 Electron impact ionization source

Besides plasma driven by a high-voltage (HV) discharge, electron impact ionization (eI^2) can also be used. Such sources are known to produce ions and other species more effectively compared to HV discharges, as the plasma is generated in a less-destructive manner. The eI^2 source employs electron bombardment of a gas pulse to induce the fragmentation and ionization of molecules (Fig. 2.9). From the pulsed valve, the gas flows through an expansion slit (3.2 cm $\times$ 50 μm) and into the vacuum chamber. A 0.2-mm diameter tungsten filament is extended along the central axis of a molybdenum tube that is slotted (through hole/slit) to expose the wire along its length. A current of 4 A through the tungsten wire heats it up and starts off the thermionic emission of electrons. Acting as a Wehnelt shield, the negatively-biased molybdenum tube confines the electron cloud along the through slit and a voltage of 80–120 V is applied to accelerate the electrons towards a grounded anode which also has an aperture to let the electron beam through. This continuous stream of electrons is placed as close as possible to the gas expansion slit and is oriented to bombard the gas pulse from below which then creates the plasma. The electron gun assembly sits on a water-cooled block to keep its temperature at an operating level. It should be noted that slit eI^2 sources have been used in the past, albeit in continuous mode (Verbraak et al. 2007). The current system described here is the first system that operates in pulsed mode, resulting in a lower gas flow that can be extended to utilize carbon-bearing precursors.

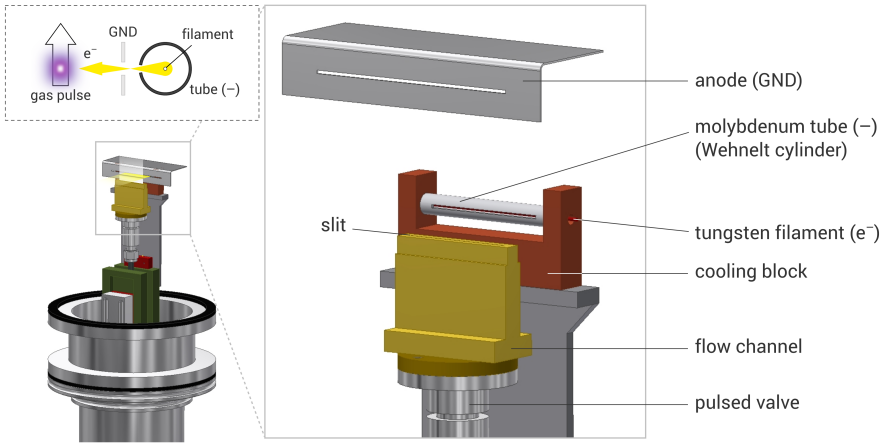

Figure 2.9: The electron impact ionization (eI^2) source as mounted on the vacuum flange. Inset cartoon: the focused electron beam hits the planar gas pulse from one side and induces plasma production. *Technical drawing by Martijn Witlox.*

2.4 Results

Presented in this section are absorption spectra as well as wide surveys of emission spectra of the hydrocarbon plasma produced using the slit discharge nozzle and the electron impact ionization source. The spectra are recorded in the visible region using IBBCEAS.

2.4.1 Optical absorption spectra of a hydrocarbon plasma

Starting from a dilute mixture of acetylene (0.3%) and argon, a hydrocarbon plasma is generated using the slit discharge nozzle and spectra are recorded through IBBCEAS. These are presented in the figures to follow and will be compared to the diffuse interstellar bands. (The simulated DIBs spectrum is based on observations done by Hobbs et al. (2009) along the sightline towards HD 183143, and each DIB is represented by a Gaussian.) In this comparison exercise, there are criteria to be fulfilled in order for a possible match to be confirmed.

First and most obvious is that the central wavelength of the absorption feature must coincide with the DIB center. Since this is an absorption measurement in the gas phase, it has the advantage of having the recorded spectra directly comparable to astronomical observations (after shifting them to the laboratory frame) in contrast to, for example, matrix isolation spectroscopy which suffers from wavelength shifts

caused by solid state interactions. It is important to ensure that laboratory data (especially in laser experiments which are measured in cm^{-1} in vacuum) are correctly compared to astronomical spectra (Å in air, which additionally requires an index of refraction scaling in view of observations done at high altitudes). Looking at Fig. 2.10a, a slight coincidence is seen between two DIBs and one of the absorption features of C_6H at around 524.7 nm. Since this band is one of the many vibronic bands of C_6H (see Chap. 4 of this thesis), it is additionally required to have a DIB aligning with the strongest band of C_6H at around 526.6 nm which is the origin band. Clearly, C_6H fails this criterion and thus, is not a DIB carrier. For this same reasoning C_8H (see Fig. 2.10b) is excluded as a DIB carrier. In the figure, there is one line coincident with a DIB absorption at a little beyond 632 nm; this is, however, excluded since it is in emission. In Fig. 2.10c a coincidence can also be observed between $C_{10}H$ and a broader DIB overlapped with narrower features. The other requirement is also fulfilled since the coincident absorption feature is the origin band of $C_{10}H$. However, this does not immediately indicate a match. Naturally, all of the subsequent vibronic bands of $C_{10}H$ that will be associated with a DIB must follow the band intensity ratios according to the assumed vibronic temperature.

If the DIB has fine structure, then the next thing to check is the band profile of the absorption feature. The shape of the band is mainly dictated by the rotational temperature of the molecules; being able to manipulate this in the laboratory is a plus. In our experimental setup, it has been shown before (see, e.g., Zhao et al. 2011a) that this is possible by adjusting the distance of the pinhole discharge nozzle from the cavity axis. Moreover, the supersonic expansion of the plasma helps produce vibrationally- and/or rotationally cool molecules which are more representative of the conditions in the astronomical environments where DIBs are observed. One can also perform CRDS measurements to fully resolve (if applicable) the rotational lines of the absorption band that will enable for the spectroscopic constants to be measured. Alternatively, band contour fitting algorithms can also be employed. These constants can then be used for simulating rotational temperatures to change the band shape accordingly.

It is natural that more questions will arise as a molecule progresses from being a potential candidate to a DIB carrier. One might then ask about the chemistry involved in the formation of the molecule. For instance, having seen (even hypothetically) an absorption feature of $C_{10}H$ in the DIBs spectrum, is it then more likely to form this larger molecule in space compared to C_8H or C_6H? If this is true, then we are taking the *top-down* route of molecule formation which is contrary to the way how we synthesize these molecules in the laboratory (i.e., starting from C_2H_2). This then poses the question whether these larger molecules can be photostable in the environments where we observe them which can also constrain certain geometries that they can have. Will cosmic rays also play a role in any of the reactions in the network leading to the formation of the molecule? If we follow the other route, *bottom-up*, then it is not possible to form $C_{10}H$ without having the smaller molecules in the mix, as what we see in our laboratory spectrum. This implies that the coincident DIB is yet caused

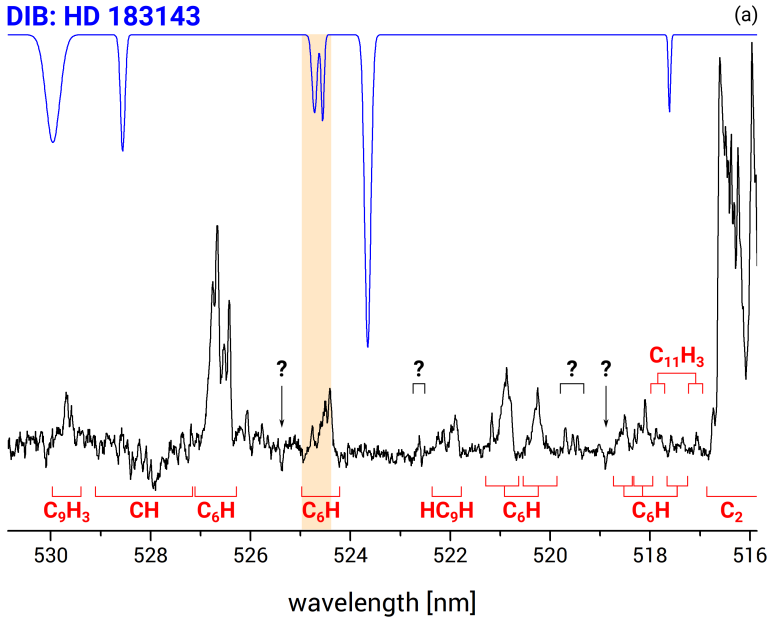
DIB: HD 183143
(a)
?
?
?
?
$C_{11}H_3$
C_9H_3
CH
C_6H
C_6H
HC_9H
C_6H
C_6H
C_2
530
528
526
524
522
520
518
516
wavelength [nm]

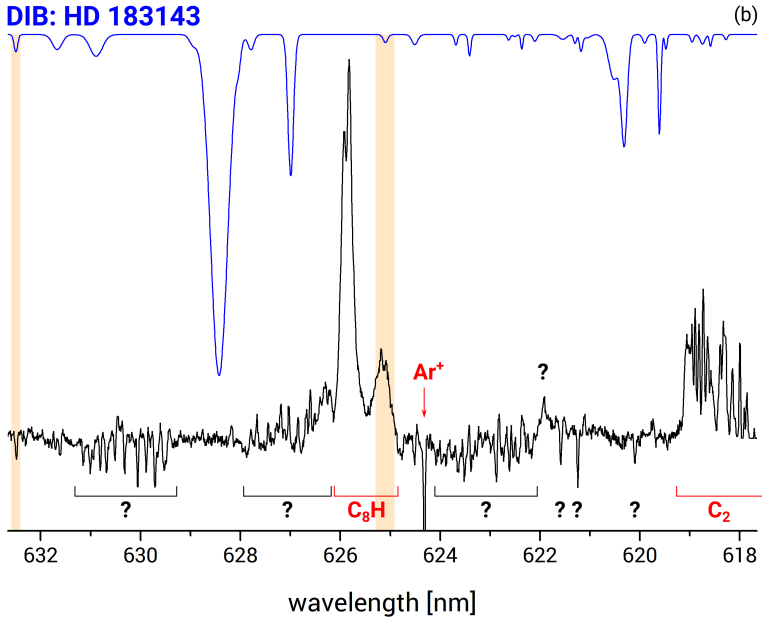
DIB: HD 183143
(b)
Ar^+
?
?
?
C_8H
?
? ?
?
C_2
632
630
628
626
624
622
620
618
wavelength [nm]

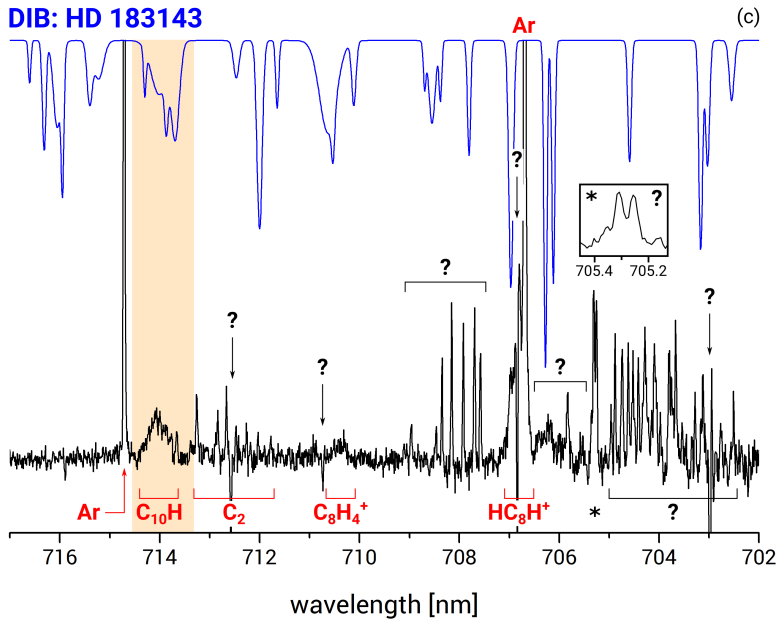

Figure 2.10: Overview spectrum of a hydrocarbon plasma measured using IBBCEAS (black trace; flipped vertically) compared to a simulated DIBs spectrum towards HD 183143 (blue trace; Hobbs et al. 2009). (a) One of the vibronic bands of C_6H (highlighted) seems to coincide – which is not necessarily a match – with a DIB feature around 524.7 nm. (b) The Ar^+ emission line at around 624.3 nm can be used for shifting the whole spectrum to rest wavelength. (c) One of the Ar absorption lines at around 706.7 or 714.7 nm can be used for shifting the whole spectrum to rest wavelength.

by another molecule with an origin- or vibronic band which happens to overlap with the origin band of $C_{10}H$. In fact, the chances are quite high, as some 500 DIBs cover the wavelength range from roughly 400–1000 nm. The process of testing continues.

There still are a few things that can be said about the laboratory spectrum. All of the spectral features, both identified[5] and unidentified, are produced simultaneously in the plasma discharge. Experimental settings, such as the discharge voltage and the backing pressure, also determine the chemical species produced in the plasma. In principle, the concentration as well as the kind of precursor gas can also be changed. These can all affect the relative amount of the species produced, so one can tune the measurement to a particular molecule. Using the different plasma sources can also

[5] All molecules indicated in the plots were identified using available wavelength positions provided for in the literature (see e.g., Motylewski et al. 2000 and references therein).

result to having diverse products, as we shall see in the emission spectra presented in the next section.

2.4.2 Optical emission spectra of a hydrocarbon plasma

By replacing the cavity mirrors of BB-DIB with MgF_2 windows, an emission spectroscopy experiment can easily be set up. Shown in Fig. 2.11 is a wide spectral survey (320–860 nm) of emission features of a hydrocarbon plasma produced with a slit discharge nozzle. Typically, a quick scan over this wavelength range takes less than 10 mins. At first glance, a number of bands can already be observed, usually in the form of vibronic progressions. These have been identified as the Swan bands of C_2 (red) and the $A^2\Delta - X^2\Pi$ transition of CH (purple). Unidentifiable features are indicated in gray.[6] Since the spacing between the rotational lines decreases as the length and/or the mass of a molecule increases, then we should expect that most of the bands that are more pronounced are due to the smaller species. Another emission feature, the electronic origin band of C_3 at ~ 405 nm is also observed (in green). The difference in the width of the band is markedly different, which means that the bands produced by larger/longer molecules would only get narrower, and thus, would require a much zoomed-in recording of spectra (such as in Fig. 2.10). We can also see individual lines that are sparsely distributed over the entire range which are likely due to atomic transitions such as that of argon and, by the fact that C_2 is produced from the dissociation of C_2H_2, hydrogen. But a significantly denser distribution of these lines can be found in the emission spectra produced by the electron impact ionization source (Fig. 2.12). Here we see the same C_2 and CH transitions as that in the slit discharge, albeit weaker (both the slit discharge and the eI^2 emission spectra are plotted with the same intensity scale).

The emission features recorded here are of less importance to DIBs research, but these may turn out useful when comparing with, for example, the extended red emission (van Winckel et al. 2002, Zagury 2009). In the figures, a relatively low-resolution spectra from the Red Rectangle nebula is superposed (blue trace; data extracted from Zagury 2009) with the hydrocarbon emission features. In a first-order inspection, none of the most prominent bands produced by the smaller species (from both plasma sources) coincide with the astronomical spectra, although at higher resolution, the $d^3\Pi_g \rightarrow a^3\Pi_u$ Swan band of C_2 has been detected (Wehres et al. 2010).

[6] It is quite possible that the unknown bands found at longer wavelengths are merely higher order diffractions of the emission features seen at much shorter wavelengths because the current configuration of the spectrograph allows for this to happen. On the CCD detector, the blue part of the higher order dispersion overlaps with the red part of the current grating order set by the spectrometer. For instance, the CH band around 430 nm shows up again at 860 nm, which is twice its wavelength. This technical issue, however, can be mitigated by using appropriate color/interference filters.

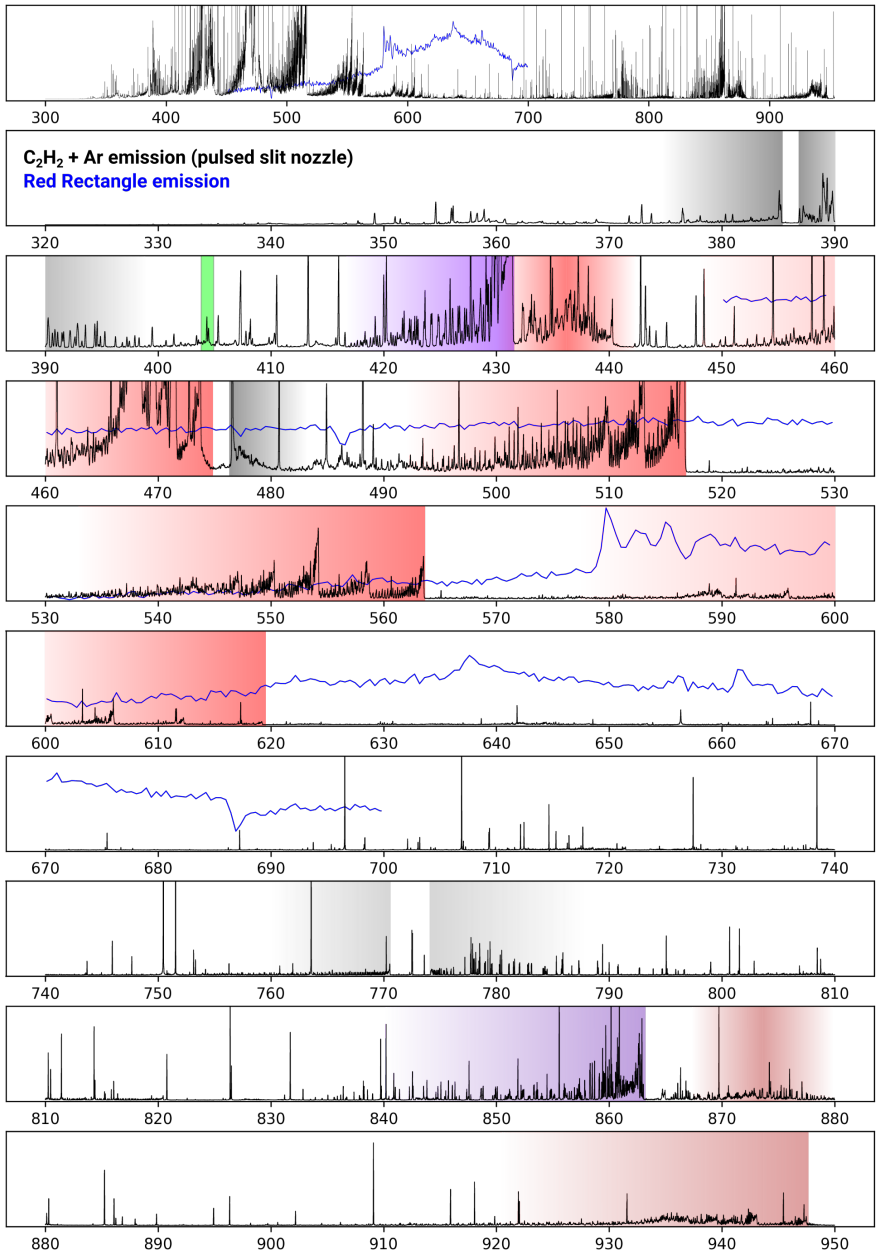

Figure 2.11: IBBCEAS wide spectral survey (320–860 nm) of emission features from the slit discharge nozzle compared with the Red Rectangle emission (Zagury 2009). See main text for a complete description.

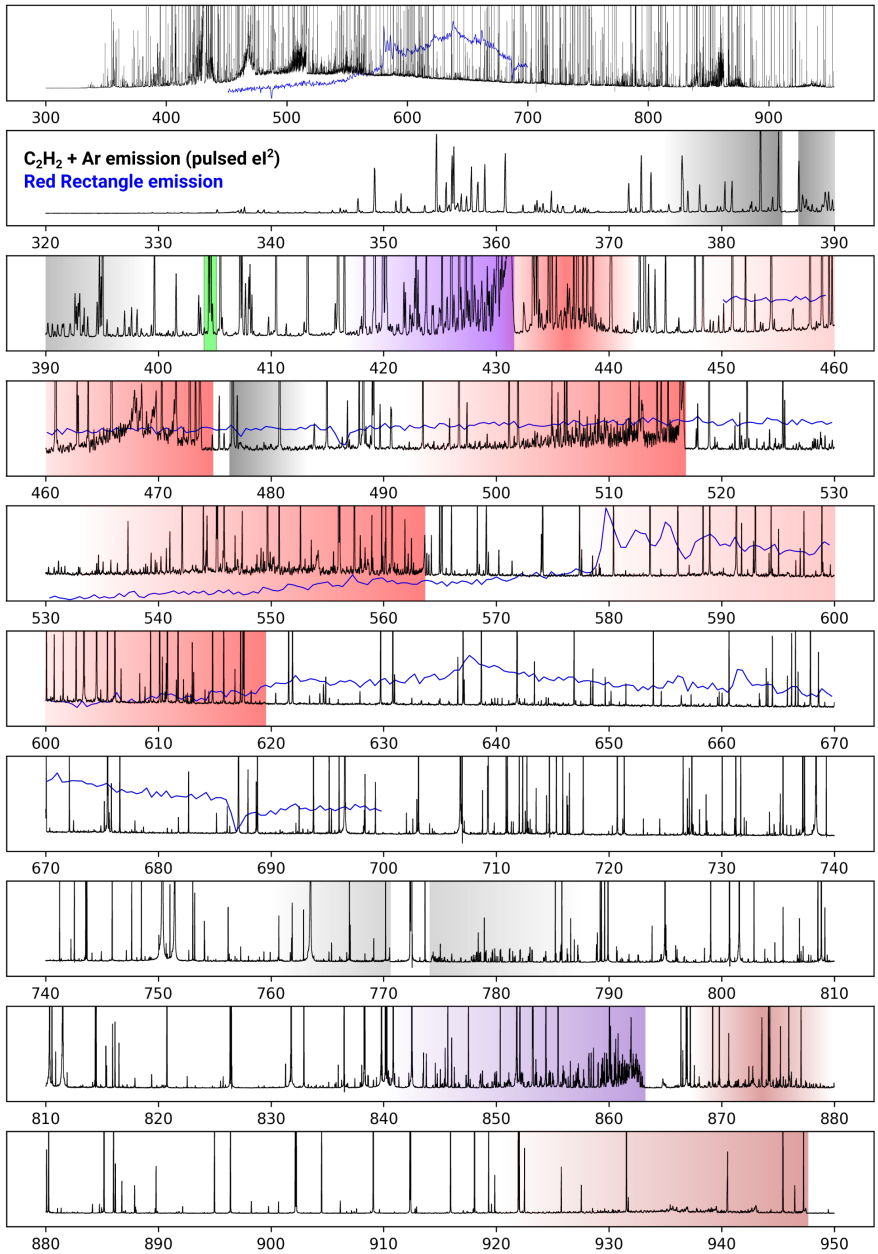

Figure 2.12: IBBCEAS wide spectral survey (320–850 nm) of emission features from the electron impact ionization source compared with the Red Rectangle emission (Zagury 2009). See main text for a complete description.

So far, we have not recorded any absorption feature of a hydrocarbon chain (e.g., C_6H, C_8H, $C_{10}H$), or of any larger molecule for that matter, using the eI^2 source in BB-DIB; these molecules can be observed with the slit discharge nozzle, as was presented in the previous section. The eI^2 source was previously operated as a continuous flow gas nozzle (Verbraak et al. 2007), and thus it was made pulsed in order to increase the density of the plasma created. This is with the assumption that the majority of the precursor molecules gets dissociated and/or ionized and can recombine through collisions. The recombination is effectively enhanced in the slit nozzle by having a small plasma interaction region in between the plates. On the other hand, since the eI^2 source produces the plasma when the gas has already started expanding into the vacuum chamber, there might well be fewer collisions taking place. Because the exact mechanism of plasma production using these sources can be challenging to pin down, one can also try out different plasma settings or even different precursor gases and check each time whether new absorption (or emission) features show up in the spectrum.

2.5 Summary

In this chapter we have presented ways as to which we can record optical absorption and emission spectra in the laboratory and have compared these measurements directly with [simulated] astronomical observations of the diffuse interstellar bands and the Red Rectangle emission. So far, no match has been confirmed. A combination of the IBBCEAS technique with high resolution spectroscopy such as CRDS holds the potential for efficiently pinning down the carriers of the DIBs. The speed of data acquisition in IBBCEAS proves to be quite useful in making spectral surveys for new bands most especially because of the almost trial-and-error nature of this experimental approach. Employing a mass-spectroscopic technique will also help in confirming the species synthesized. In addition, using hydrocarbon precursors other than acetylene in combination with the newly-developed pulsed electron impact ionization source as well as the slit plasma nozzle will be a way forward in searching for new spectral features in the laboratory.